Resonance Raman Spectroscopic and Density Functional Theory Study of Benzoin Diethyl Phosphate

Wing Sum Chan, Chensheng Ma, Wai Ming Kwok, Peng Zuo, and David Lee Phillips*

Department of Chemistry, The University of Hong Kong, Pokfulam Road, Hong Kong S.A.R., P. R. China

Received: September 17, 2003; In Final Form: January 5, 2004

Raman spectra of benzoin diethyl phosphate (BDP) have been obtained in resonance with two different electronic states using excitation at 252.7 and 354.7 nm in acetonitrile solvent. Extensive overtone and combination bands of the carbonyl C═O stretching (1700 cm^{-1}) and carbonyl attached ring C═C stretching (1597 cm^{-1}) vibrations were observed in the 252.7 nm spectrum. Density functional theory (DFT) calculations were made to determine the structure and the vibrational modes and frequencies for the ground state of BDP. Vibrational bands observed in the resonance Raman spectra were assigned using the DFT results, and it was found that modes showing a strong enhancement in the Raman spectra were mainly related to the benzoinyl moiety, especially the acetophenone subgroup. This was corroborated by the DFT calculated molecular orbitals. Our results indicate that 354.7 and 252.7 nm excitation corresponds to electronic transitions from the ground state to the nπ^* and $\pi\pi^*$ states, respectively. We briefly discuss the implications of these results in understanding the mechanism of the BDP deprotection reaction.

Introduction

There has been much attention focused on the photochemical reactions of benzoin esters because of their ability to undergo rapid photolysis with high efficiency that leads to the generation of a single inert byproduct in addition to a free acid.[1−4] The practical properties of these compounds have led to the development of the parent benzoinyl chromophore and its substituted analogues as photoremovable protecting groups for a variety of common functional groups.[5−8] For example, Givens et al. investigated the photodeprotection of biologically activate substrates (such as phosphates, nucleotides, amino acids, etc.) from the corresponding desyl caged ester.[3,7−10] The biochemically benign product was produced with high efficiency and yield, and the photodeprotection reaction occurs with rate constants of $\sim 10^8-10^9$ s^{-1}.[4,7] The photodeprotection reactions of these benzoin esters occur much faster than reactions of commonly used *o*-nitrobenzyl analogues that have typical rates of reaction of 1−100 s^{-1}.[3,7,11] This faster deprotection of benzoin ester compounds is important because it allows one to study the kinetics of related biochemical events and provides a unique way to monitor the rapid and localized activation of biological receptors.

An investigation of the pathway for the photodeprotection reaction is essential in describing the relevant photochemical processes and developing new functional groups for use in photodeprotection reactions. Previous studies on the photochemistry of benzoin and its substituted analogues showed that the reaction pathway and efficiency are highly dependent on both the nature of the solvent and the type of substituent group attached to the phenyl ring.[1,2,4,12−14] In solvents such as acetonitrile, the photodeprotection process is accompanied by some photocyclization to form a corresponding 2-phenylbenzofuran product. The highest yield for the photocyclization occurs for compounds with meta-methoxy substitution.[1,2,13] However, the yield of benzofuran (the photocyclization product) was found to decrease substantially for benzoin diethyl phosphate (BDP) and its analogues in aqueous environments or in solvents with high ionizing ability such as 2,2,2-trifluoroethanol (TFE) and hexafluoro-2-propanol (HFP).[4,7,14] Depending on the properties of the leaving group and the aryl substituents, substantially different reaction mechanisms have been proposed to interpret the experimental observations. On the basis of nanosecond and picosecond laser flash photolysis (LFP) and excited-state Stern−Volmer quenching experiments, Givens et al. suggested a triplet mechanism for the photodeprotection of BDP.[4,7] However, by using the LFP combined with oxygen/nitrogen purge experiments, Wan et al. proposed a singlet mechanism for the cleavage reactions of various 3′,5′-dimethoxybenzoin esters.[12] Work done by Sheehan et al.[2] and Pirrung et al.[13] provides some support for a singlet mechanism. In addition to the issue of the multiplicity of the state where the bond cleavage takes place, some other mechanisms and their corresponding transient intermediates have been proposed to be involved in the overall deprotection reaction. For instance, direct heterolytic cleavage of the ketone α-C−O bond,[13] homolytic cleavage followed by electron transfer,[4,7] biradical formation followed by acetoxy migration,[14] and intramolecular exciplex formation accompanied by heterolytic cleavage[12] have all been suggested to explain the deprotection cleavage process in several molecular compounds.

The mechanism and reactivity of a photoexcited state can be understood in terms of the difference in the electron density distribution of the excited state compared to that of its ground state. Such a difference in the electron density can be inferred from the change in structure that the molecule undergoes upon going from the ground to the excited state. We note that despite the extensive studies done for a variety of benzoin ester phototrigger compounds there have been few if any vibrational studies performed to obtain direct structural information for the ground and excited states.[15] Time-resolved vibrational experiments enable real-time detection and monitoring of the dynamics

* Author to whom correspondence should be addressed. E-mail: phillips@hku.hk. Fax: 852-2857-1586.

10.1021/jp036774u CCC: $27.50
Published on Web 04/14/2004

of short-lived transient species.[16,17] Thus, time-resolved vibrational spectroscopy is an ideal method to help elucidate photochemical reaction mechanisms. For phenyl ketones, it has been shown that the nature of the lowest excited state and the interaction between the nearby lowest excited states, normally the $\pi\pi^*$ and $n\pi^*$ nature states, have a significant effect on the photochemical reactivity of these compounds.[18−21] Our long-term program seeks to obtain direct experimental evidence for the explicit identification of the photoexcited intermediates and the establishment of the related dynamical conversions from which we can construct a more comprehensive view of the reaction mechanism(s) involved in deprotection reactions. We hope that such studies will better help to explain the photochemistry of benzoin ester phototrigger compounds. Herein, we report use of resonance Raman spectroscopy to investigate the structural and electronic properties of both the ground state of BDP and the initial excited state formed following either 252.7 or 354.7 nm photoexcitation.

The utility of employing Raman spectroscopy to help determine molecular structure is well known, and resonance Raman spectroscopy has been recognized to be a valuable technique to use in obtaining information about the excited state potential surface in the Franck−Condon (FC) region of the ground state.[22−43] The intensity distribution of the resonance Raman bands can provide important information regarding the molecular structure and properties of the excited electronic state.[22,36−38,42] The resonance enhancement pattern can also contain information about the nature of the vibronic interaction between nearby excited states.[22,39−41,43] To help elucidate the nature of excited states and the possible interaction between them, resonance Raman spectra of ground state BDP have been obtained in resonance with two different electronic states—the so-called ring $\pi\pi^*$ (S_3) and carbonyl $n\pi^*$ (S_1) states—using excitation wavelengths of 252.7 and 354.7 nm, respectively. A simple model and calculation were made to simulate the absorption spectrum and resonance Raman intensities for the 252.7 nm excitation. This calculation was also used to estimate the possible preresonance contribution from the strong S_3 $\pi\pi^*$ state to the 354.7 nm spectrum, which is expected to derive its resonance Raman intensities from the weak S_1 $n\pi^*$ state. Density functional theory (DFT) calculations were also performed to determine the ground-state geometry and to help make vibrational assignments for the experimental vibrational spectra. We found that modes exhibiting strong enhancements in the resonance Raman spectra were largely linked to the benzoinyl moiety, especially the acetophenone subgroup. This is consistent with the DFT calculated molecular orbitals. We briefly discuss these results in relation to understanding the initial stages of the mechanism of the photodeprotection reaction and related processes in BDP. The vibrational spectra, DFT calculations, and vibrational assignments also provide background information that is needed to perform time-resolved vibrational spectroscopic experiments on BDP and other benzoin deprotection compounds in the future.

Experimental and Computational Methods

BDP was synthesized following the method suggested in ref 7. The identity and purity of the BDP sample were confirmed by analyzing NMR, UV absorption, and mass spectrometric spectra. Spectroscopic-grade acetonitrile solvent was used as received to prepare the BDP sample solutions.

A normal Raman spectrum of solid phase BDP was obtained using a Renishaw Raman microspectrometer employing 514 nm excitation from an Ar ion laser. An FT-IR spectrum of BDP was recorded using a Bio-Rad FTS/64 FT-IR spectrometer with the sample encased in solid KBr windows. The spectral resolution was approximately 5 cm^{-1} for both the Raman and IR spectra of BDP. A steady state absorption spectrum of BDP in acetonitrile was measured using an HP 8453 UV spectrometer with 1 nm resolution.

Resonance Raman experiments were done using an experimental apparatus described previously.[36−38] Excitation wavelengths of 354.7 and 252.7 nm were used for the experiments. The 354.7 nm excitation wavelength was supplied by the third harmonic of a Spectra Physics GCR-150-10 Nd:YAG Q-switched laser. The 252.7 nm excitation wavelength came from the third anti-Stokes hydrogen Raman shifted line pumped by the fourth harmonic (266 nm) of the Nd:YAG laser. The excitation energy for each excitation wavelength was in the 0.5−2 mJ range with a repetition rate of 10 Hz. The laser beam was focused slightly onto the sample, and the Raman light was collected in a backscattering configuration and detected by a liquid nitrogen cooled CCD detector. A circulated acetonitrile solution with a sample concentration of ~2 mM was used to acquire the 252.7 nm resonance Raman spectrum. Because of the weak absorption at around 355 nm, a quartz cell that contained the sample solution of ~95 mM was used for the 354.7 nm experiments. To ensure that a fresh sample was exposed to each excitation laser pulse, the sample cell was kept moving during the 354.7 nm experiments by a 2D translation stage. The spectra were accumulated over 10 min. The resonance Raman spectra were intensity corrected for any remaining reabsorption by the sample and the wavenumber dependence of the detection system's response. The solvent bands were removed from the resonance Raman spectra by subtracting an appropriately scaled solvent-only spectrum from the resonance Raman spectrum. The known vibrational frequencies of the solvent acetonitrile Raman bands were used to calibrate the resonance Raman spectra with an estimated accuracy of ±5 cm^{-1} in absolute frequency. Values of the depolarization ratio for the resonance Raman bands bearing significant intensity were measured for both of the excitation wavelengths. The integrated Raman band areas were found by fitting a portion of the Raman spectrum to a baseline plus the sum of the Lorentzian bands. The absolute Raman cross sections were determined with reference to the published values of the Raman cross sections of the acetonitrile solvent bands.[44−46]

A time-dependent methodology[22] was used to fit the absorption spectrum for the strong S_3 state and the corresponding resonance Raman cross sections at both 252.7 and 354.7 nm wavelengths. The time-dependent wave packet calculations have been used to analyze the resonance Raman intensities for many other compounds,[24,36−38,45,46] and a detailed description of these types of calculations can be found in refs 22, 24, 36, and 38.

The optimized geometry and vibrational frequencies were obtained from B3LYP density functional theory (DFT) calculations employing the cc-PVZD basis set and C_1 symmetry. No imaginary frequency modes were observed for the optimized structure. The DFT Raman and IR activities were also calculated to allow for direct comparison with the experimental spectra. Time-dependent DFT computations for the random-phase approximation (RPA) were made to estimate the vertical electronic transition energy and corresponding oscillator strengths. This combined with calculated frontier molecular orbitals was used to help interpret the resonance enhancement pattern observed in the resonance Raman spectra and to study the extensive conformational change induced by photoexcitation. All of the calculations were made using the Gaussian 98 program suite.[47]

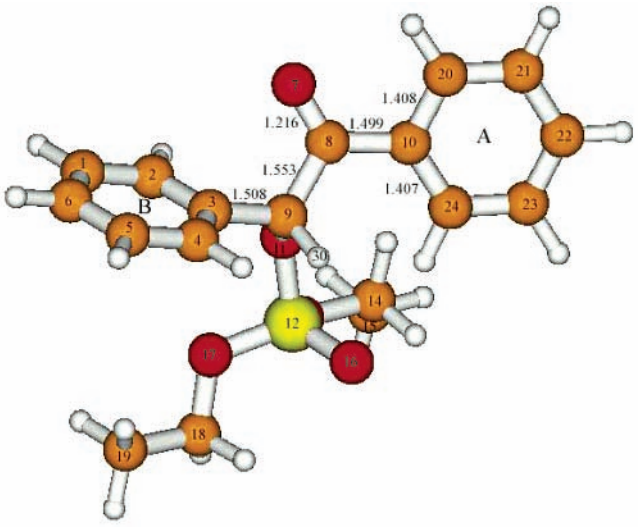

Figure 1. Optimized structure of the BDP ground state obtained from B3LYP/cc-PVZ DFT calculations.

TABLE 1: Structural Parameters of the BDP Ground State Found from the B3LYP/cc-PVZ DFT Calculations

bond length (Å)		bond angle (deg)		dihedral angle (deg)	
C1−C2	1.395	O7−C8−C9	120	C9−C3−C4−C5	178.6
C1−C6	1.4	O7−C8−C10	121.4	C2−C3−C9−C8	72.8
C2−C3	1.402	C9−C8−C10	118.6	C2−C3−C9−O11	−44
C3−C4	1.4	C3−C9−C8	113.5	C2−C3−C9−H30	−164.5
C3−C9	1.508	C3−C9−O11	111.5	C4−C3−C9−C8	−105.8
C4−C5	1.399	C3−C9−H30	109.6	O7−C8−C9−C3	−19.1
C5−C6	1.397	C8−C9−O11	103.8	C10−C8−C9−C3	161.4
O7−C8	1.217	C8−C9−H30	109.5	O7−C8−C10−C20	1.9
C8−C9	1.553	O11−C9−H30	108.7	C9−C8−C10−C24	0.8
C8−C10	1.499	C8−C10−C20	117.1	C3−C9−O11−P12	−95.8
C9−O11	1.461	C8−C10−C24	123.6	C8−C9−O11−P12	141.6
C10−C20	1.408	C20−C10−C24	119.3	H30−C9−O11−P12	25.2
C10−C24	1.407	C9−O11−P12	118.5	C8−C10−C20−C21	179.1
O11−P12	1.636	O11−P12−C13	101.5		
P12−C13	1.623				
P12−C16	1.503				
P12−C17	1.619				
C13−C14	1.454				
C14−C15	1.515				
C17−C18	1.454				
C18−C19	1.515				
C20−C21	1.393				
C21−C22	1.401				
C22−C23	1.398				

Results

A. Optimized Geometry and Vibrational Analysis of BDP. Figure 1 displays the optimized geometry found from B3LYP/cc-PVDZ calculations for the BDP ground state. Selected structural parameters are given in Table 1. Experimental normal Raman and FT-IR spectra of BDP in the 500−1800 cm^{-1} region are shown in Figure 2a and c, respectively. Calculated B3LYP/cc-PVDZ Raman and IR spectra based on the optimized structure are also presented in Figure 2b and d, respectively, for comparison to the experimental spectra. A Lorentzian function with a 10 cm^{-1} bandwidth was used to produce vibrational bands for the calculated spectra in Figure 2. Table 2 provides a summary of the experimental and calculated vibrational frequencies and vibrational assignments made from a direct comparison between the experimental and calculated spectra. The calculated vibrational frequencies were scaled by a factor of 0.9688. This scaling value minimizes the root-mean-square difference between calculated and experimental frequencies for bands with definitive or known identification. Vibrational coupling was found to be quite extensive for most vibrational modes. The assignments are partially based on the atomic displacements of the calculated normal mode, and the descriptions listed in Table 2 include only vibrations with predominant contributions to the corresponding vibrational modes.

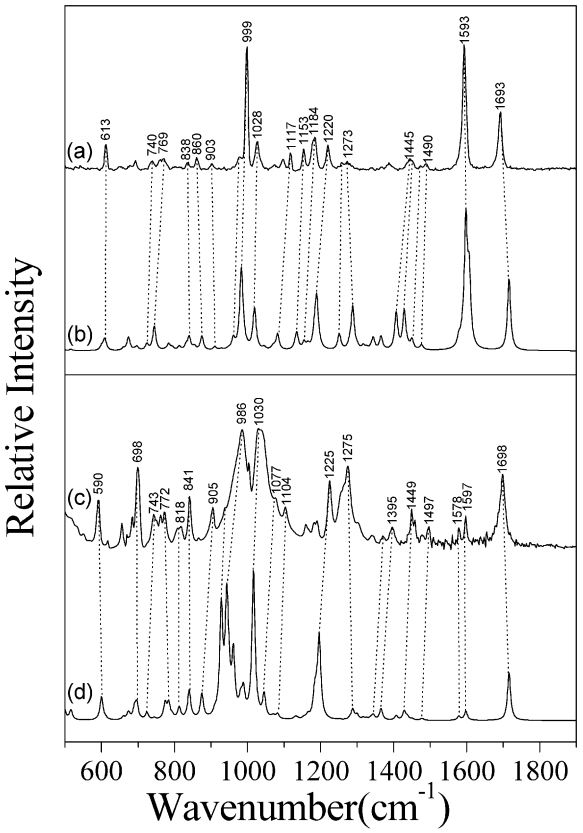

Figure 2. Experimental and DFT calculated normal Raman (a, b) and IR (c, d) spectra in the 500−1800 cm^{-1} region for the ground state of BDP. See the text for more details.

The two phenyl rings have an almost regular hexagon structure with the C−C−C angles very close to 120° and a mean C−C distance of ∼1.4 Å. The 179.1, 1.9, and 0.8° dihedral angles for O8−C10−C20−C21, O7−C8−C10−C20, and C9−C8−C10−C24, respectively, indicate that the carbonyl group and the carbon bridge (C10−C8−C9) are close to the plane of the ring with the carbonyl attached to it (ring A in Figure 1). The dihedral angle of C9−C3−C4−C5 is 178.6°, and this implies that C9 is also in the plane of ring B. (See Figure 1.) The torsion angle between the two rings was found to be ∼72.8° as indicated by the C2−C3−C9−C8 dihedral angle listed in Table 1. From the bond length data, one can find that the C8−C10 bond, connecting the carbonyl group and ring A, has a length (1.499 Å) shorter than a typical C−C single bond length (such as the 1.515 Å bond length calculated for the C18−C19 bond). This along with the planarity of the carbonyl group with ring A indicates that the carbonyl group interacts noticeably with the π electrons in the attached ring. We note that, like the C8−C10 bond, the C9−C3 bond also has a shorter-than-normal C−C single bond length and the bridging C9−C8 bond has a longer-than-normal C−C single bond length.

To our knowledge, there is no X-ray diffraction data published for this compound for comparison to the optimized geometry. However, an inspection of Figure 2 shows that the experimentally observed Raman and IR spectra agree reasonably well with the B3LYP/cc-PVDZ computed spectra. This implies that the

TABLE 2: Observed and Calculated Vibrational Frequencies (cm^{-1}) and Assignment for Ground State BDP

experimental		calculated		
Raman	IR	frequency		assignment descriptions
	590	ν95	600	CCC bending (ring B > A) + C(8)−C(9) stretching (minor)
613	617	ν93	611	CCC bending (ring B)
654	656	ν92	660	CCC bending (ring A) + C−C stretching (C(8)−C(9/10) + ring B)
679	684	ν91	674	ring A boat def. + P−O(11) stretching + C(8)−C(9/10) stretching
693	698	ν89	696	C−H bending (o.p., ring A)
740	743	ν88	724	C−H bending (o.p., ring B) + P−O(11/13/17) stretching
[a]	750	ν87	744	C−H bending (o.p., ring B > A) + P−O(13/17) stretching
762	762	ν86	774	H bending (o.p., ring A)
769	772	ν85	784	P−O(13/17) stretching + C−O(13/17) stretching + C(15/19)H3 wag + C(18)H2 rock
807	808	ν83	794	C(18 > 14)H2 rock + C(19 > 15)H3 wag
	818	ν82	812	C−C stretching (ring B > A + C(3/9/8/10)
838	841	ν80	840	C−H bending (o.p., ring B) + P−O(11) stretching + C(9)−C(3/8) stretching
860		ν79	854	C−H bending (o.p., ring A)
903	905	ν78	875	P−O(11) stretching + C−O(11) stretching + C(9)−C(3/8) stretching + C−C stretching (ring A, minor)
	937	ν76	928	C(14/18)-C(15/19) stretching
	[a]	ν75	943	C(14/18)-C(15/19) stretching + C−O(13/17) stretching + P−O(13/17) stretching + C−H bending (o.p., ring A, minor)
	[a]	ν74	948	C−H bending (o.p., ring A)
979	[a]	ν72	961	C−O(11) stretching + C−H bending (o.p., ring A)
	986	ν70	981	C−C stretching (all except diethyl group) + C−O(11) stretching + P−O(11) stretching (minor)
999	[a]	ν69	983	C−C stretching (all except diethyl group)
	[a]	ν67	989	C−C stretching (all except diethyl group) + C−O(11) stretching + P−O(11) stretching (minor)
	1003	ν65	1016	C(14/18)-C(15/19) stretching + C−O(13/17) stretching + P−O(13/17) stretching
1028		ν63	1019	C−C stretching (ring A > B)
	1030	ν62	1045	C(14/18)−C(15/19) stretching + C−O(11/13/17) stretching + P−O(13/17/11) stretching + P═O stretching (minor)
	1077	ν61	1068	C−H bending (i.p., ring B) + C−C stretching (ring B)
1075	1077	ν60	1072	C−H bending (i.p., ring A) + C−C stretching (ring A)
1097		ν59	1082	C(18)−C(19) stretching + C(19)H3 wag + C−O(17) stretching
1097		ν58	1082	C(14)−C(15) stretching + C(15)H3 wag + C−O(13) stretching
1117	1104	ν57	1129	C(14)H2 rock + C(15)H3 rock
1117	1104	ν56	1130	C(18)H2 rock + C(19)H3 rock
1153		ν55	1134	C−H bending (i.p., ring B)
1153	1160	ν54	1135	C−H bending (i.p., ring A)
1184	1183	ν53	1154	C−H bending (i.p., ring B)
1184		ν52	1165	C−H bending (i.p., ring A)
	1190	ν51	1183	P═O(16) stretching + C−(30) bending + C−C stretching (ring A + C(8)−C(9/10)) + P−O(11/13/17) stretching + C−H bending (i.p., ring B, minor)
1220	1225	ν49	1196	C−C stretching (all except diethyl group) + C−H bending (i.p., both ring)
1258	[a]	ν48	1250	C(18)H2 twist + C(19)H3 wag
[a]		ν47	1252	C(14)H2 twist + C(15)H3 wag
1273	1275	ν45	1288	C−C stretching (C(3/9/8/10)) + C−H(30) bending + C−H bending (i.p., both ring, minor)
	1302	ν44	1299	C−C stretching (ring A + C(8)−C(9/10)) + C−H bending (i.p., ring A + C−H(30))
1338	1344	ν39	1344	C−C stretching (ring B + C(9)−C(3/8)) + C−H bending (i.p., ring B + C−H(30))
1367[b]	1370[b]	ν38	1365	C(14/18)H2 wag + C(15/19)H3 wag + C(14/18)−C(15/19) stretching
1387[b]	1395[b]	ν36	1406	C(19)H3 scissor
1445[b]		ν34	1428	C(15)H3 scissor + C(14)H2 scissor (minor)
	1449*b*	ν33	1429	C(19)H3 scissor + C−H bending (i.p., ring B) + C(18)H2 scissor (minor)
1453[b]		ν32	1429	C(19 > 15)H3 scissor + C(18)H2 scissor (minor)
	1459	ν31	1437	C−C stretching (ring B) + C−H bending (i.p., ring B)
1474	1478	ν29	1451	C(14)H2 scissor
1490	1497	ν28	1475	C−C stretching (ring A + C(8)−C(10)) + C−H bending (i.p., ring A)
1490	1497	ν27	1478	C−C stretching (ring B + C(3)−C(9)) + C−H bending (i.p., ring B)
	1578	ν26	1578	C−C stretching (ring A + C(8)−C(10)) + C═O(7) stretching (minor)
1593	1597	ν24	1597	C−C stretching (ring A + C(8)−C(10))
1693	1698	ν22	1716	C═O(7) stretching (major) + C(8)−C(9/10) stretching
2930	2932	ν19	2947	C(15)H3 stretching (sym.) + C(14)H2 stretching (sym.)
2930	2932	ν18	2947	C(19)H3 stretching (sym.) > C(18)H2 stretching (sym.)
2978	2984	ν14	3022	C(15)H3 stretching
2978	2984	ν13	3023	C(15)H3 stretching
	3034	ν12	3031	C(15)H3 stretching + C(14)H2 stretching (asym.)
	3034	ν11	3033	C(19)H3 stretching > C(18)H2 stretching
3068	3069	ν7	3085	C−H stretching (ring A)
3068	3069	ν6	3086	C−H stretching (ring B)

[a] Unresolved shoulder bands. [b] Bands with uncertain assignments.

optimized structure obtained from the B3LYP/cc-PVDZ calculations is reasonable, and this makes assignments of the vibrational bands relatively straightforward. Thus, the carbonyl C═O stretching vibrational mode (∼1700 cm^{-1}) and most modes related to the ring C−C stretching and C−H bending vibrations are readily assigned as shown in Table 1. However, some vibrational modes, especially those appearing in the 1000−1150 and 1300−1450 cm^{-1} regions that have predominant contribu-

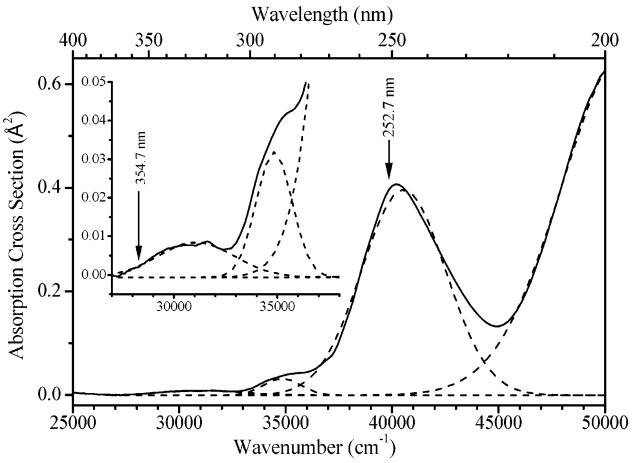

Figure 3. Experimental absorption spectrum (—) of BDP in acetonitrile solution. Gaussian deconvolution (- - -) of the absorption spectrum.

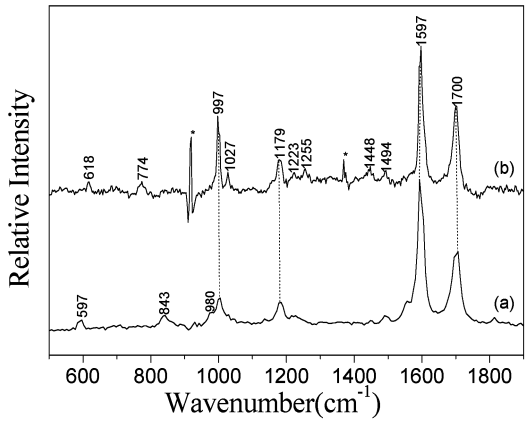

Figure 4. Resonance Raman spectra of BDP obtained with excitation at 252.7 nm (a) and 354.7 nm (b) wavelengths in acetonitrile solvent. The concentrations used for the measurements are ~2 and ~95 mM for 252.7 and 354.7 nm excitation, respectively. The asterisks (*) mark solvent subtraction artifacts.

tions related to the diethyl phosphate group, are not predicted as well by the B3LYP/cc-PVDZ calculation results. The assignments of these vibrational bands are therefore known with somewhat less certainty. (These bands are denoted by footnote b in Table 2). Fortunately, few of these bands appear in the resonance Raman spectra; therefore, the uncertainties of their assignments do not significantly influence the interpretation of our resonance Raman spectra obtained for BDP.

B. Resonance Raman Spectra of BDP. Figure 3 shows a steady state absorption spectrum of BDP recorded in acetonitrile solution. The spectrum is displayed with the *x* axis in units of both energy (cm^{-1}) and wavelength (nm) and the *y* axis in units of the absorption cross section ($Å^2$).[22] It can be seen that the absorption spectrum displays a strong band with a maximum at ~250 nm (ϵ = 11 610 L mol^{-1} cm^{-1}) and two smaller partially overlapping weak bands in the ~280−305 nm (ϵ = 2141 L mol^{-1} cm^{-1}) and ~305−380 nm (ϵ = 1216 L mol^{-1} cm^{-1}) regions. (See also the inset of Figure 3.) We tentatively designate the three bands as being due to electronic transitions from $S_0 \rightarrow S_3$, $S_0 \rightarrow S_2$, and $S_0 \rightarrow S_1$, respectively. With reference to the UV absorption spectra of the related benzoin ester and phenyl ketones reported in the literature,[1,13,18,56] the three absorption bands can be correlated with phenyl ring dominated $\pi\pi^*$ transitions for the ~260 nm (L_a) and ~280−305 nm (L_b) bands and the carbonyl dominated $n\pi^*$ transition for 305−380 nm absorption. In acetonitrile solvent, the photoexcitation of BDP leads to the formation of the final product benzofuran within ~10 ns (i.e., the duration of the excitation laser pulse).[4] Benzofuran absorbs in the 260−330 nm region and has strong fluorescence in the 300−400 nm region.[4,57] This makes it very difficult to nearly impossible to measure a Raman excitation profile of BDP though such information would be valuable to obtain so as to provide a better understanding of the excited state profile and the extent of mixing between the lowest excited states. To avoid the final product absorption band, 252.7 and 354.7 nm excitation wavelengths (as indicated by arrows in Figure 3) were chosen carefully for the resonance Raman experiments. It is clear from Figure 3 that the two excitation wavelengths lie in the strong L_a and weak $n\pi^*$ electronic transitions, respectively. Attempts using excitation wavelengths resonant with the L_b electronic transition failed because of overwhelming fluorescence from the benzofuran final product.

Figure 4 displays the resonance Raman spectra of BDP (in 500−1800 cm^{-1} region) obtained using the 252.7 and 354.7 nm excitation wavelengths. The two spectra are normalized to the same intensity for the common strongest band at 1593 cm^{-1}, although the absolute intensity of the 354.7 nm resonance Raman spectrum is actually rather weak because of its weak absorption strength. (See Figure 3.) Resonance Raman bands that appear in 500−1800 cm^{-1} region are most probably fundamental bands, and their assignments can be tentatively made from comparison to the normal Raman spectrum and to the vibrational analysis discussed earlier. (See also Table 2.) The vibrational frequencies of the observed resonance Raman bands along with their assignments and the values of the depolarization ratio when measurable are listed in Table 3. Solvent effects probably account for the small differences in frequency found for the corresponding Raman bands recorded in the solid state (from the normal Raman spectrum listed in Table 2) and in acetonitrile solution. At both excitation wavelengths, no clear feature was seen below 500 cm^{-1}. The 354.7 nm resonance Raman spectrum shows no band above 1800 cm^{-1}. However, extensive overtone and combination bands were observed in the high wavenumber region for the 252.7 nm resonance Raman spectrum. A full spectrum covering the 0−5500 cm^{-1} region along with tentative assignments of the observed bands is presented in Figure 5. Similar spectra were observed in a mixed acetonitrile/water solvent system.

It is clear that the same main Raman band features—1700, 1597, 1179, and 997 cm^{-1}—are observed at both excitation wavelengths. The 1700 cm^{-1} band corresponds to the carbonyl C═O stretching mode. The 1597 and 1179 cm^{-1} bands are assigned, respectively, to the C═C stretching (the Wilson 8a) and C−H in-plane bending (Wilson 9a) modes of ring A. The 997 cm^{-1} band corresponds to a strongly coupled mode with major contributions from the C−C stretching of rings A and B and the carbon bridge between them. Several common weak features at 1494, 1448, and 1223 cm^{-1} are observed at both excitation wavelengths. The relative intensities of the features are somewhat different in the two spectra. The 997 cm^{-1} band and the C═O stretching mode both display substantially more resonance enhancement in the 354.7 nm spectrum than in the 252.7 nm spectrum. Other weak bands at 980, 843, and 597 cm^{-1} appear only in the 252.7 nm spectrum, and the 1255, 1027, 774, and 618 cm^{-1} bands appear only in the 354.7 nm spectrum. An examination of Table 3 shows that the three weak features at 1448, 1255, and 774 cm^{-1} are associated with vibrations related to the diethyl phosphate leaving group. All of the other Raman bands appear to be mainly associated with vibrations from the benzoin subgroup. This indicates that excitation using

TABLE 3: Frequencies and Assignment of Vibrational Bands Observed in Resonance Raman Spectra of BDP Obtained with 252.7 and 354.7 nm Excitation

resonance Raman[a]		calculation		
252.7-nm excitation	354.7-nm excitation	frequency		assignment descriptions
597		ν95	600	CCC bending (ring B > A) + C(8)−C(9) stretching (minor)
	618	ν93	611	CCC bending (ring B)
	774	ν85	784	P−O(13/17) stretching + C−O(13/17) stretching + C(15/19)H3 wag + C(18)H_2 rock
838		ν80	840	C−H bending (o.p., ring B) + P−O(11) stretching + C(9)−C(3/8) stretching
979		ν72	961	C−O(11) stretching + C−H bending (o.p., ring A)
1002 (0.39)	997 (0.30)	ν69	983	C−C stretching (all except diethyl group)
	1027	ν63	1019	C−C stretching (ring A > B)
1182 (0.33)	1179	ν52	1154	C−H bending (i.p., ring A)
1227	1223	ν49	1196	C−C stretching (all except diethyl group) + C−H bending (i.p., both rings)
	1255	ν48	1250	C(18)H2 twist + C(19)H3 wag
1444[b]	1448	ν33	1429	C(19)H3 scissor + C−H bending (i.p., ring B) + C(18)H_2 scissor (minor)
1488	1494	ν28	1475	C−C stretching (ring A + C(8)−C(10)) + C−H bending (i.p., ring A)
1597 (0.36)	1597 (0.58)	ν24	1597	C−C stretching (ring A + C(8)−C(10))
1701 (0.36)	1700 (0.30)	ν22	1716	C═O(7) stretching (major) + C(8)−C(9/10) stretching
1814		ν95 + ν49		
1992		2ν69		
2594		ν69 + ν24		
2699		ν69 + ν22		
2778		ν53 + ν24		
2881		ν53 + ν22		
3196		2ν24		
3301		ν24 + ν22		
3390		2ν22		
4301		ν69 + ν24 + ν22		
4380		2ν22 + ν69		
4799 (0.38)		3ν24		
4905 (0.36)		2ν24 + ν22		
4993 (0.35)		3ν22		

[a] Values of measured depolarization ratios are indicated in parentheses. [b] Band with uncertain assignment.

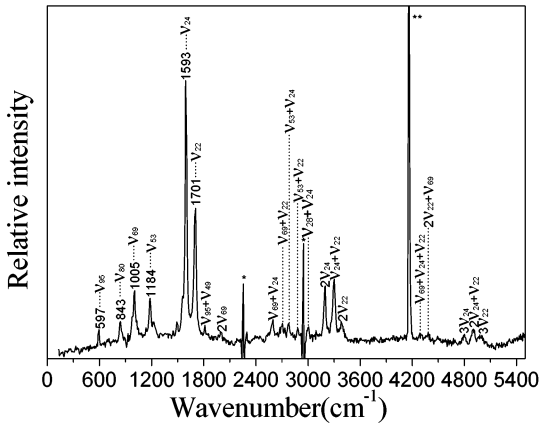

Figure 5. Resonance Raman spectrum of BDP in acetonitrile solution obtained with 252.7-nm excitation (2 mM concentration). The asterisk (*) marks solvent subtraction artifacts. The double asterisk (**) marks bands due to scattering from laser lines.

the 252.7 and 354.7 nm excitation wavelengths leads to distortion mainly along the vibrational modes associated with the benzoinyl chromophore with only a little perturbation to the phosphate group.

An inspection of Figure 5 shows that in addition to fundamental Raman bands the 252.7 nm resonance Raman spectrum also displays significant intensity in overtone progressions up to third order for the ring C═C stretching 8a (ν_{24}) and carbonyl C═O stretching (ν_{22}) modes. The spectrum also displays intense combination bands between these two modes and combination bands of these modes with other resonance-enhanced modes (such as the ν_{69}, ν_{53}, and ν_{28} modes). However, the 354.7 nm resonance Raman spectrum displays no discernible intensity in overtone or combination bands.

As the Raman excitation frequency approaches an electronic resonance, the observed enhancements of vibrational Raman scattering are often analyzed under the assumption that the enhancements arise solely from the electronic state(s) with which the excitation is resonant. However, several examples have been reported that indicate the importance of resonance−preresonance interference in determining the fundamental Raman intensities in some molecular systems. This type of preresonance effect could noticeably perturb the fundamental intensities even when the preresonance transition is fairly far away in energy. Because the S_1 state in BDP is intrinsically weak and somewhat close in energy to the strong S_3 state, it is essential to estimate the possible preresonance contribution of the latter state to the 354.7 nm resonance Raman intensity. To do so, we have used a time-dependent wave packet model to simulate simultaneously the absorption spectrum of the strong S_3 state and the experimentally measured absolute Raman cross sections obtained with 252.7 nm excitation. With the same set of parameters, we also calculated the Raman cross sections for fundamentals at the 354.7 nm excitation wavelength and compared this result with the experimentally obtained cross sections.

Table 4 presents the fit parameters for the simulations and comparison between the calculated and experimental absolute Raman cross sections for both excitation wavelengths. Figure 6 (top) displays a comparison of the calculated S_3 absorption spectrum with the experimental spectrum and its Gaussian deconvolution. Figure 6 (bottom) also shows a comparison of the computed absolute Raman cross sections with the experimental values for the 10 fundamentals and 11 overtones and combinations observed in the 252.7 nm resonance Raman spectrum. The results in Figure 6 show that there is reasonable agreement between both the absorption and resonance Raman calculated and experimental cross sections for the 252.7 nm

TABLE 4: Parameters for Simulations of the Resonance Raman Cross Section and Absorption Spectrum of BDP in Acetonitrile Solvent and a Comparison of the Calculated and Experimental Raman Cross Sections for the 252.7 and 354.7 nm Excitation Wavelengths[a]

				absolute Raman cross section (Å^2)			
				252.7-nm excitation		354.7-nm excitation	
	S_0 freq (cm^{-1})	S_3 freq (cm^{-1})	Δ	calcd ($\times 10^{-9}$)	exptl ($\times 10^{-9}$)	calcd ($\times 10^{-11}$)	exptl ($\times 10^{-11}$)
ν_{95}	597	597	0.06	1.04	1.58	0.00	
ν_{80}	838	838	0.14	6.74	7.50	0.01	
ν_{72}	979	979	0.1	3.61	4.13	0.00	
ν_{69}	1002	1002	0.22	17.54	18.25	**0.02**	**7.51**
ν_{53}	1182	1182	0.22	17.72	18.40	0.03	
ν_{49}	1227	1227	0.12	5.26	5.47	0.01	
ν_{33}	1444	1444	0.18	11.62	12.07	0.02	
ν_{28}	1488	1488	0.08	2.29	3.14	0.01	
ν_{24}	1597	1597	0.574	117.50	115.28	**0.29**	**12.47**
ν_{22}	1701	1600	0.497	83.14	82.22	**0.19**	**10.52**
$\nu_{24} + \nu_{69}$	2599			3.83	7.58	0.00	
$\nu_{22} + \nu_{69}$	2703			2.72	3.34	0.00	
$\nu_{24} + \nu_{53}$	2779			4.19	5.01	0.00	
$2\nu_{24}$	3194			15.24	16.46		
$\nu_{24} + \nu_{22}$	3298			21.70	20.04		
$2\nu_{22}$	3402			9.30	10.78		
$\nu_{22} + \nu_{24} + \nu_{69}$	4300			0.75	1.79		
$2\nu_{24} + \nu_{69}$	4376			0.58	1.80		
$3\nu_{24}$	4791			1.42	3.98		
$2\nu_{24} + \nu_{22}$	4895			3.03	7.97		
$3\nu_{24}$	4999			2.60	5.72		

[a] $E_0 = 40\,100$ cm^{-1}, $M = 0.855$ Å, $n = 1.344$, homogeneous broading $\Gamma = 1650$ cm^{-1}, HWHM inhomogeneous broading $G = 340$ cm^{-1}.

spectrum. The measured values of the depolarization ratio of the vibrational modes observed with 252.7 nm excitation are all in the range of 0.3−0.4. (See Table 3.) Because these values are close to the $^1/_3$ theoretical value, these depolarization ratios indicate that Raman bands shown in the 252.7 nm spectrum derive their scattering cross section predominantly from the S_3 state. As also seen in Table 4, the calculated Raman cross-section values at 354.7 nm coming from the S_3 absorption are more than 50 times smaller than the experimental ones, implying that the preresonance contribution of the S_3 state to the 354.7 nm resonance Raman spectrum is negligibly small. This is consistent with the values of ∼0.3 for depolarization ratios of the 997 and 1701 cm^{-1} bands in the 354.7 nm spectrum (Table 3) and suggests that the enhancement of these two modes originates predominantly from the weak S_1 state. However, we note that the depolarization ratio of the strongest 1597 cm^{-1} feature in the 354.7 nm spectrum (Figure 4b) is measured to be ∼0.58 (Table 4), and this indicates an additional source contributing to its intensity. This 1597 cm^{-1} mode is a symmetric ring C═C stretching vibration, and we attribute its large 0.58 depolarization ratio to the preresonance−resonance effect from the nearby and partially overlapped S_2 state of $\pi\pi^*$ nature, as indicated by our DFT molecular orbital calculation. (See below.)

For most aromatic carbonyl compounds, the weakly allowed character of the S_1 $n\pi^*$ transition has been suggested to be due to the vibrational coupling of this state with the nearby $\pi\pi^*$ state(s) through out-of-plane torsional vibrations related to the ring-attached carbonyl group. These torsional vibrations are typically observed at frequencies lower than 200 cm^{-1}.[61] Because both of the resonance Raman spectra obtained here (Figures 4 and 5) show no recognizable features below 300 cm^{-1}, we conclude that the modes responsible for the vibrational coupling are not detected here but could be detected by scanning the Raman excitation through the lowest three absorption bands. Although we intended to do so, these resonance Raman experiments were hindered by very prompt and strong fluores-

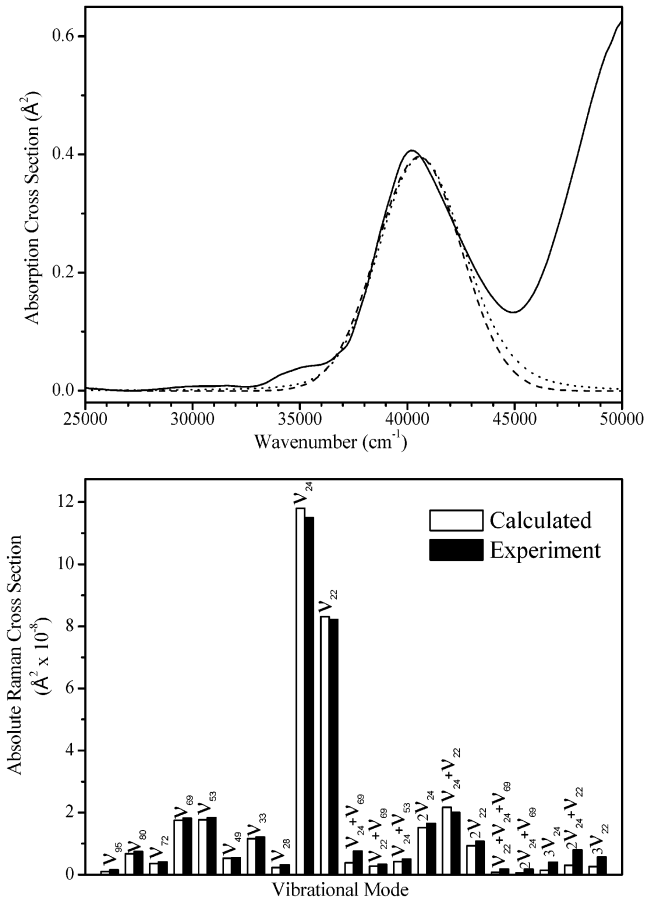

Figure 6. (Top) Comparison of the calculated absorption spectrum (• • •) with the experimental (—) and Gaussian deconvolution (- - -) absorption spectra. (Bottom) Comparison of the calculated resonance Raman cross sections (open bars) with experimental values (solid bars) observed in the 252.7 nm resonance Raman spectrum shown in Figure 5. The calculation makes use of the parameters listed in Table 4 and the model described in ref 22.

TABLE 5: Electronic Transition Energies, Oscillator Strengths, and Related Molecular Orbital Transitions Obtained from B3LYP/cc-PVZ DFT Calculations for the BDP Ground State

	$S_0 \rightarrow S_1$	$S_0 \rightarrow S_2$	$S_0 \rightarrow S_3$
excitation energy[a]	342.66 nm (0.0012)	289.46 nm (0.0143)	246.71 nm (0.2852)
	92 → 93 (0.46037)	91 → 93 (0.57746)	88 → 93 (0.46887)
molecular	90 → 93 (0.41112)	92 → 93 (0.38764)	89 → 93 (0.40762)
orbital changes[b]	91 → 93 (−0.23557)		89 → 94 (0.11702)
	89 → 93 (−0.12895)		

[a] Numbers in parentheses are oscillator strengths of the corresponding excitations. [b] Numbers in parentheses are contributions of the corresponding orbital changes to the excitations.

cence and absorption from the photoproduct (as described before), and an alternative method is needed to address this point in the future.

The large degree of resonance Raman intensity at both excitation wavelengths for the vibrational modes associated with the carbonyl C═O stretching (1700 cm^{-1}), the ring modes (1597 and 1179 cm^{-1}), and the vibration involving the C−C bridge (997 cm^{-1}) mode indicates that there are significant displacements along these modes upon the excitation of the $S_0 \rightarrow S_1$ (354.7 nm) and $S_0 \rightarrow S_3$ (252.7 nm) electronic transitions. (See Table 4.) The substantial intensity in the overtones and combinations associated with the C═O and ring C═C modes in the 252.7 nm resonance Raman spectrum indicates the existence of fairly large S_3-S_0 displacements along these two coordinates. The displacement of S_1 relative to S_0 is expected to be much smaller along the carbonyl C═O and ring C═C stretching coordinates because no overtone or combination bands for these two modes were observed in the 354.7 nm resonance Raman spectrum associated with the $S_0 \rightarrow S_1$ electronic transition. The larger degree of enhancement of the 997 cm^{-1} band with $S_0 \rightarrow S_1$ excitation compared to that with $S_0 \rightarrow S_3$ excitation implies that S_1 excitation leads to more changes in the bonding on the C−C bridge than does S_3 excitation. This suggests that the conformational distortion of the desyl subgroup, especially the C═O and carbonyl-connected ring moiety, is fairly large upon excitation. This is consistent with previous experimental and theoretical findings that many aryl carbonyl compounds show extensive structural deformation of the carbonyl moiety and phenyl ring in excited singlet and triplet states with respect to the ground state.[48,50−56]

We note that the weak shoulder on the Raman band at 980 cm^{-1} that appears in the 252.7 nm spectrum has some contribution from the C9−O11 bond stretching vibration. (See Table 3.) The stretching of this bond will eventually lead to cleavage of the phosphate leaving group from the caged part of the system. The weakness of this band and the absence of any other bands in the resonance Raman spectra related to the cleavage motion rule out any direct photodissociation pathway for the BDP photodeprotection reaction. The cleavage step therefore must occur later on after excitation through an intermediate that could conceivably be the singlet state outside the Franck−Condon region or more likely the lowest triplet state of BDP or some other intermediate that has not yet been established explicitly.[1,2,4,7,12−14]

Information on the instantaneous change in the electronic configuration induced by an electronic transition is important to the interpretation of the structural change observed upon photoexcitation and is also helpful in understanding the enhancement pattern observed in resonance Raman spectroscopy. Time-dependent DFT calculations were made with the random-phase approximation (RPA) to estimate the vertical transition energies, oscillator strengths, and changes in molecular orbitals involved in the electronic transitions. This method has been found to give reasonable estimates for transitions to low-lying excited states for various molecules.[57−59] Table 5 shows the predicted lowest three absorption bands obtained from these time-dependent DFT calculations for BDP, and these results can be compared to the experimental absorption spectra given in Figure 3. The relevant frontier molecular orbitals related to the three electronic transitions obtained from the time-dependent DFT calculations for BDP are displayed in Figure 7. Compared with the UV absorption spectra shown in Figure 3, the calculated excitation energies and oscillation strengths are in reasonable agreement and consistent with the experimental absorption bands.

The lowest unoccupied molecular orbital (LUMO, orbital 93) has clear antibonding π^* character and resides on both the carbonyl moiety and its attached phenyl ring (ring A) group; some π bonding character can be seen for the C8−C10 bond connecting phenyl ring A and the carbonyl group. The highest occupied molecular orbital (HOMO, orbital 92) appears to have similar contributions from the carbonyl oxygen lone pair and the π bonding electron of the unattached phenyl ring system (ring B). Orbital 90 (HOMO-2) has contributions from mostly the carbonyl oxygen lone pair with a small contribution from the antibonding π^* of ring B. Orbitals 89 (HOMO-3) and 88 (HOMO-4) both have π bonding character of ring A, and orbital 91 (HOMO-1) has a π bonding orbital of ring B.

According to the TD-RPA (DFT) calculations (Table 5), excitation to the S_1 state is mainly a transition combination of LUMO ← HOMO with 0.46 weight and LUMO ← HOMO − 2 with 0.41 weight. Given the character and nature of the three orbitals, such a transition will lead to the promotion of electron density from the carbonyl oxygen lone pair to the antibonding π^* orbital of the carbonyl and ring A group; a moderate bonding change in ring B and the C−C bridge is also expected. The S_1 state can thus be viewed broadly as an $n\pi^*$ state, in general agreement with its previous assignment.[1,13] Subsequent conformational changes that result from this transition occur obviously at the desyl group, which leads to a substantial lengthening of the carbonyl C8−O7 bond and some expansion of the attached ring A accompanied by some shortening of the C8−C10 bond. These predicted changes in geometry upon S_1 excitation are fully consistent with the 354.7 nm resonance Raman spectrum and give a good explanation of the strong Raman intensity appearing in the 1700 cm^{-1} C═O stretching, the 1593 cm^{-1} ring-stretching, and 997 cm^{-1} desyl skeleton stretching vibrational modes.

The S_2 state is formed from the transition combination LUMO ← HOMO and LUMO ← HOMO − 1 with contributions of 0.39 and 0.58, respectively. This excitation is predominantly a transformation of electron density from the π bonding orbital of ring B to the antibonding π^* LUMO orbital. It is therefore $\pi\pi^*$ in nature. The oscillator strength of this transition is small because of small orbital overlap.

The $S_0 \rightarrow S_3$ excitation has contributions from LUMO ← HOMO − 3 (0.41 weight) and LUMO ← HOMO − 4 (0.47 weight) transitions, leading to the promotion of a ring A bonding

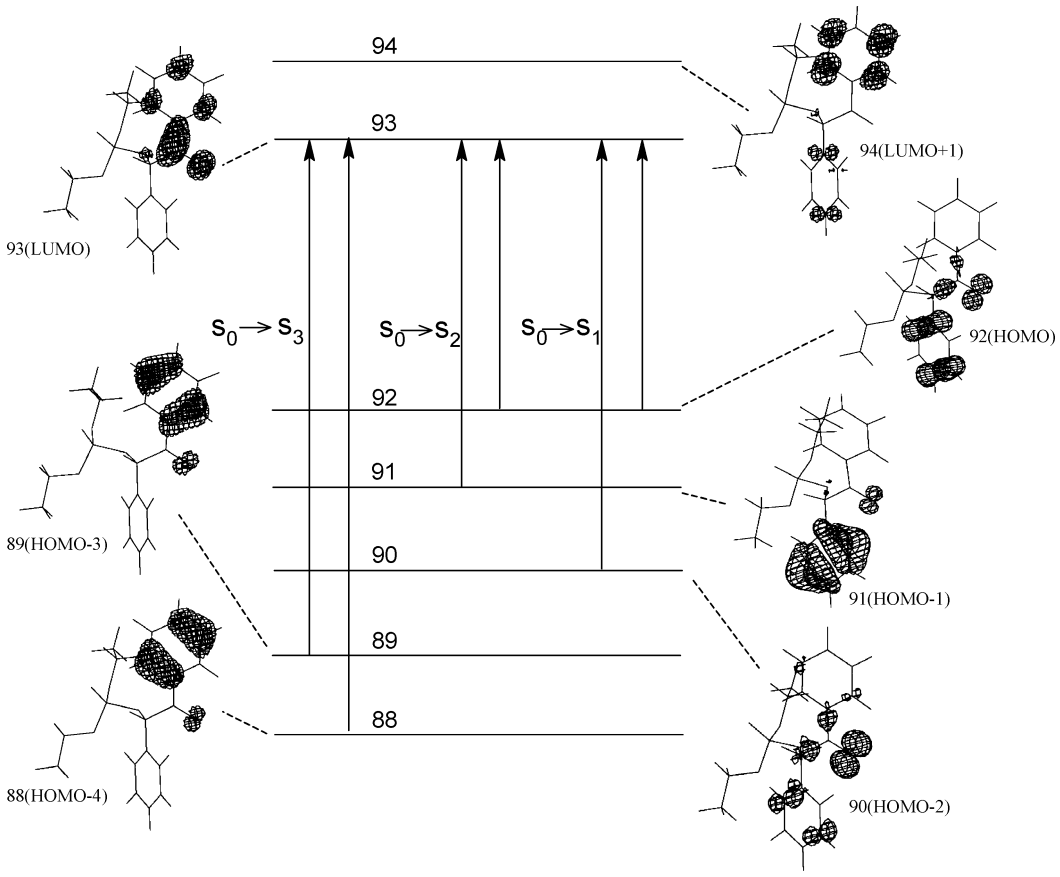

Figure 7. Frontier molecular orbitals for the ground state of BDP obtained from B3LYP/cc-PVZ DFT calculations.

π electron to an antibonding π^* LUMO orbital. This excitation is mostly localized on the benzoinyl carbonyl group. The S_3 state can accordingly be taken as a $\pi\pi^*$ state in line with the general assignment of this state reported in the literature.[18,48] Such a change in the electronic configuration is expected to have a large oscillator strength as predicted by the RPA calculation. This transition results in a substantial weakening of ring A and the carbonyl bonding π system, which is fully consistent with the extensive overtone and combinations of the ring 1597 cm^{-1} C−C stretching and 1700 cm^{-1} carbonyl C−O stretching modes observed in the 252.7 nm resonance Raman spectrum. From Table 5 and Figure 5, it can be seen that all of the relevant frontier molecular orbitals have little contribution from the diethyl phosphate leaving group. This explains the absence of obvious resonance Raman bands related to the vibration of the phosphate group in the 252.7 and 354.7 nm resonance Raman spectra.

Discussion

The structural and electronic changes that occur in an excited state molecule play a decisive role in determining the photochemical behavior. Our results here that are based on resonance Raman spectra in conjunction with molecular orbital calculations provide clear evidence that both $n\pi^*$ and $\pi\pi^*$ excitation of BDP leads to substantial conformational changes in the carbonyl and ring groups (especially ring A). The excitation of these electronic transitions leads to a lengthening of the carbonyl C−O bond and a substantial expansion of the ring size; consequently, the equilibrium conformations of the two states are significantly different from the ground state geometry. The $\pi\pi^*$ excitation leads to change localized on the acetophenone subgroup, and the $n\pi^*$ excitation makes noticeably more change in the C−C bridge bond and the ring B system. Our present results also shows that the slope of $\pi\pi^*$ (S_3) potential surface is much large than that for the $n\pi^*$ (S_1) state in the FC region along the relevant normal modes. These are expected to have important implications for the photochemistry of BDP.

The cyclization and nucleophilic reactions of BDP (mentioned in the Introduction) have been found to be mostly complete within 25 ns.[4] These cyclization and nucleophilic reactions can also be mostly quenched by typical triplet state quenchers, and the BDP triplet state has been suggested to be the common precursor for both types of reactions.[4] However, the mechanism for these cyclization and nucleophilic reactions is still unclear and is being debated.[2,4,12−14] DFT calculations by us[60] and theoretical work by others[49] have shown that phenylbenzofuran possesses a planar structure. As described above, the ground state BDP has nonplanar structure in terms of the orientation of the acetophenone subgroup, the C−C bridging bond, and unconjugated ring B. The ring B system is twisted 72.8° out of the plane formed by the acetophenone and C−C bridge subgroups. From a stereospecific point of view, this implies that a large-amplitude torsional motion (most probably a twisting of ring B) must occur to bring the three parts into a same plane at some point along the reaction pathway. Calculated molecular orbital configurations show that because of increased conjugation interaction the carbonyl carbon atom will stay at the attached ring plane after photoexcitation. However, the carbonyl oxygen atom could deviate from this plane.[55,56] Even with this taking place, for the cyclization to occur, the torsion of ring B around the C3−C9 bond may still be needed to allow the 2′ carbon to approach the carbonyl oxygen atom. It is known that torsional vibrations are normally in the low-frequency range (∼100−300 cm^{-1}).[61] In our resonance Raman spectra, the

absence of any obvious feature at frequencies below 500 cm^{-1} indicates that such a mode does not appear to contribute significantly to either the $\pi\pi^*$ (S_3) or $n\pi^*$ (S_1) transition. The cyclization, though rapid, is therefore not induced directly by photoexcitation of the three low-lying transitions. The cyclization reaction could result from the BDP triplet[4,7] and might accompany or take place after the cleavage of the phosphate leaving group in the deprotection reaction.[2,12,14]

The effect of water on BDP photolysis pathways is intriguing. In aqueous solution, cyclization is prevented in a significant fraction of the photoproduct, accompanied by the generation of an additional solvent nucleophilic substitution product.[4,7,14] This means that (i) the nucleophilic reaction can compete effectively with the cyclization reaction and (ii) the benzylic carbon must be accessible to nucleophilic attack by water at a certain point along the photolysis reaction pathway. Our present results show that the resonance Raman spectra exhibit no obvious difference in acetonitrile, and the mostly aqueous acetonitrile solvent implies that the processes observed exclusively in water does not occur immediately after photoexcitation. It could proceed through the triplet state as suggested by Givens et al.[4,7] or some other intermediate proposed by others.[14] Several experimental results have been presented in the literature favoring a heterolytic cleavage mechanism for BDP and/or other benzoin ester compounds. For example, the heterolytic cleavage product α-keto cation has been suggested to be responsible for a transient absorption at 570 nm observed for the photoexcitation of BDP in a mostly aqueous environment and also in a TFE solvent.[4] These solvents of high ionizing ability have been known to encourage heterolytic dissociation through preferentially stabilizing the ion pair produced.[62−64] It appears that this special solvent effect plays a crucial role in controlling the reaction pathway for BDP and related compounds. The elucidation of the details of this reaction mechanism and the identification of intermediate(s) involved in it will be a subject for a number of research groups including us.

In contrast to the triplet mechanism proposed for BDP, the photochemistry of several ring-substituted benzoin compounds, such as 3′, 5′- dimethoxybenzoin, has been attributed to a singlet reaction based on the observation that the cyclization reaction is not quenched to any appreciable extent by a triplet quencher or oxygen.[2,12] In addition, it has been found that the cyclization efficiency is considerable larger for 3′, 5′- dimethoxybenzoin than for unsubstituted benzoin compounds such as BDP.[1,2,13] The quantum yields of the corresponding benzonfuran cyclization product are measured to be ∼0.63 and ∼0.1−0.15 for 3′,5′-dimethoxybenzoin ester and unsubstituted benzoin esters, respectively.[1,2] One possible interpretation is the following. Provided that the photoproduct and general rapid ISC rate for aromatic carbonyl compounds are the same (direct measurement of the ISC rate for benzophenone indicates that its singlet has a lifetime of $\sim 1.6 \times 10^{-11}$s),[65] the triplet mechanism may be generally applicable to the photoreaction of both the substituted and unsubstituted benzoin compounds. The reaction of both types of compounds could proceed from the triplet state, and the different observation in the triplet quenching experiments may reflect only the fact that the reaction of the 3′,5′-dimethoxybenzoin ester is faster than the diffusion-controlled limit of quenching ($\sim 10^{-10}$ s) whereas that of the unsubstituted benzoin ester compounds is slower than the diffusion rate. An alternative interpretation is also possible. The two types of molecular systems follow mechanisms of different multiplicity, as suggested in the literature.[2,4,12,13] Extensive work on the photochemistry of aromatic carbonyl compounds shows that their photochemical outcomes can be highly sensitive to both the nature of the solvent and the type of substituent group attached to the phenyl ring.[19−21,66,67] This is especially true for compounds with the $n\pi^*$ and $\pi\pi^*$ states lying close in energy, which appears to be the case for BDP and related molecules.

Discussions of the photoreactivity of BDP from either the proposed triplet or singlet mechanisms in the literature assume that an excited state with of $n\pi^*$ nature is a precursor for the reactions based on indirect evidence.[2,4,7,12] This appears to be rather reasonable especially in terms of the fact that the cyclization reaction is favored by the presence of a properly situated electron donor (the $-OCH_3$ group as mentioned above) that is consistent with the electrophilic nature of the $n\pi^*$ carbonyl state. However, despite the BDP $n\pi^*$ singlet (S_1) being much lower in energy than the $\pi\pi^*$ singlet (S_3) as shown in the ground state absorption spectrum of Figure 3, our present results indicate that the potential energy surface of the $\pi\pi^*$ state has a larger slope than that of the $n\pi^*$ state. This suggests that before reaching the equilibrium position the energy gap between the two states decreases along the relevant common coordinate-(s) and it may be possible that the two surfaces come close to one another or even meet at certain point along these coordinates. This can influence the ISC rate and the dynamics and possibly the mechanism of the photochemical reaction. The energy separation between a triplet state and its counterpart singlet state is normally larger for $\pi\pi^*$ states than for $n\pi^*$ states.[68] Taking into considering the fact that the energy levels of the $\pi\pi^*$ and $n\pi^*$ states exhibit a different dependence on solvent polarity,[19−21,68] the $\pi\pi^*$ and $n\pi^*$ triplet states of BDP are thus expected to be only an approximate estimate of the energy, and their order may be sensitive to the nature of the solvent environment. Our DFT calculations using the same method and basis set as used here for the ground state of BDP found a triplet state of $\pi\pi^*$ nature. The major conformational difference between this triplet state and the ground state occurs at the acetonphenone and C−C bridge part of the molecule. The relative orientation of ring B with ring A and the geometric parameters related to ring B and the phosphate leaving group are similar in both of these states. The carbonyl C8−O7 bond is lengthened by ∼0.1 Å, and the C−C bond connecting the carbonyl moiety and the ring (C8−C10) is shortened by ∼0.06 Å in the triplet state relative to the ground state. Other changes include a shortening of the C−C bridge (C9−C8) by 0.04 Å and a lengthening of the ring A C10−C24 and C10−C20 bonds by ∼0.02 Å. It is interesting that these structural changes are consistent with the expected changes induced by direct $\pi\pi^*$ excitation (S_3). If the ISC rate is rapid, then further picosecond time scale experimental work is probably needed to detect the triplet state and determine its possible role in the deprotection reaction mechanism. A straightforward way to distinguish and establish the nature of the BDP triplet state is to measure its carbonyl C═O stretching frequency and make a comparison with the 1700 cm^{-1} ground state frequency as observed here. Such experiments have not yet been reported for BDP, but we plan to do this soon. From previous Raman and IR studies on aromatic carbonyl compounds, it has been found that the CO group of a $\pi\pi^*$ state basically retains its double bond nature and downshifts of the vibrational mode frequency relative to the ground state are typically only ∼100 cm^{-1}. In contrast, the CO group of $n\pi^*$ triplet state has mainly single bond character and lies at a much lower vibrational frequency in the ∼1200−1300 cm^{-1} range.[51−54]

Previous investigations have found that the photochemistry of some aromatic carbonyl compounds exhibits a strong

dependence on the excitation energy and the nature of the excited-state reached by photoexcitation.[66,67] For instance, the $S_0 \rightarrow S_1$ ($n\pi^*$ transition) excitation of gas phase benzaldehyde results in free radical formation whereas the $S_0 \rightarrow S_2$ ($\pi\pi^*$ transition) excitation leads to an intramolecular process resulting in the generation of benzene and CO.[66] It was also suggested that for phenyl ketones possessing nearby $n\pi^*$ and $\pi\pi^*$ triplet states the two states would mix strongly and the photoreaction may take place from an equilibrium population of the two states.[19] $S_0 \rightarrow S_1$ $n\pi^*$ excitation has been utilized intentionally in several previous studies to investigate the photochemistry of BDP and related compounds.[2,12,14] It was found that both the cyclization and nucleophilic reactions occur following the excitation of this type of electronic transition. However, a recent time-resolved transient absorption study found that both the $S_0 \rightarrow S_1$ $n\pi^*$ and $S_0 \rightarrow S_1$ $\pi\pi^*$ excitations could be used to monitor the kinetics of the BDP reaction and complex dynamical processes were observed on the nanosecond time scale.[4] This suggests that further work is needed to elucidate better the possible influence of the excitation energy on the photochemistry of BDP and related compounds.

Conclusions

We have reported resonance Raman spectra of BDP obtained in acetonitrile with excitation in its $n\pi^*$ and $\pi\pi^*$ states at 354.7 and 252.7 nm wavelengths, respectively. DFT calculations have been made to determine the structure and vibrational frequencies for the ground state of the BDP molecule. The observed resonance Raman bands were assigned on the basis of the DFT results. The excitation energies and molecular orbitals were also computed to compare with and interpret the resonance enhancement of the experimental resonance Raman spectra. It was found that modes exhibiting strong enhancements are mainly related to the benzoinyl moiety for both excitation wavelengths and the $\pi\pi^*$ state is localized on the acetophenone subgroup. Only fundamentals are observed for the 354.7 nm resonance Raman spectrum obtained with $n\pi^*$ excitation. However, pronounced overtone and combination band progressions of the carbonyl C═O stretching at 1700 cm^{-1} and carbonyl attached ring C═C stretching at 1597 cm^{-1} were observed for the 252.7 nm resonance Raman spectrum obtained with $\pi\pi^*$ excitation. This means that along the coordinates corresponding to these two vibrational modes there exist fairly large potential surface displacements between the $\pi\pi^*$ excited state and the ground state. However, there is only a relatively small displacement between the $n\pi^*$ excited state and the ground state, so only fundamentals were observed in the 354.7 nm resonance Raman spectrum. This is expected to influence not only the ISC rate but also the mechanism of the photochemistry of BDP. The absence of resonance Raman bands in the resonance Raman spectra related to the cleavage motion of the diethyl phosphate group rules out any direct photodissociation pathway for the BDP photodeprotection reaction. The results reported here also provide a foundation for future time-resolved vibrational spectroscopic investigations of the reaction mechanisms for the photochemistry of BDP.

Acknowledgment. D.L.P. thanks the Research Grants Council of Hong Kong (HKU 7108/02P) for financial support. W.M.K. thanks the University of Hong Kong for the award of a Postdoctoral Fellowship.

References and Notes

(1) Sheehan, J. C.; Wilson, R. M. *J. Am. Chem. Soc.* **1964**, *86*, 5277−5281.
(2) Sheehan, J. C.; Wilson, R. M.; Oxford, A. W. *J. Am. Chem. Soc.* **1971**, *93*, 7222−7228.
(3) Givens, R. S.; Kueper, L. W., III. *Chem. Rev.* **1993**, *93*, 55−66.
(4) Rajesh, C. S.; Givens, R. S.; Wirz, J. *J. Am. Chem. Soc.* **2000**, *122*, 611−618.
(5) Rock, R. S.; Chan, S. I. *J. Org. Chem*. **1996**, *61*, 1526−1529.
(6) Cameron, J. F.; Willson, C. G.; Frechet, J. M. J. *J. Am. Chem. Soc.* **1996**, *118*, 12925−12937.
(7) Givens, R. S.; Athey, P. S.; Matuszewski, B.; Kueper, L. W., III; Xue, J. Y.; Fister, T. *J. Am. Chem. Soc.* **1993**, *115*, 6001−6012.
(8) Givens, R. S.; Athey, P. S.; Kueper, L. W., III; Matuszewski, B.; Xue, J. Y. *J. Am. Chem. Soc.* **1992**, *114*, 8708−8710.
(9) Givens, R. S.; Matuszewski, B.; Athey, P. S.; Stoner, M. R. *J. Am. Chem. Soc.* **1990**, *112*, 6016−6021.
(10) Givens, R. S.; Matuszewski, B. *J. Am. Chem. Soc.* **1984**, *106*, 6860−6861.
(11) Park, C. H.; Givens, R. S. *J. Am. Chem. Soc.* **1997**, *119*, 2453−2463 and references therein.
(12) Shi, Y. J.; Corrie, J. E. T.; Wan, P. *J. Org. Chem*. **1997**, *62*, 8278−8279.
(13) Pirrung, M. C.; Shuey, S. W. *J. Org. Chem*. **1994**, *59*, 3890−3897.
(14) Rock, R. S.; Chan, S. I. *J. Am. Chem. Soc.* **1998**, *120*, 10766−10767.
(15) Pawelka, Z.; Kryachko, E. S.; Zeegers-Huyskens, T. *Chem. Phys*. **2003**, *287*, 143−153.
(16) Kwok, W. M.; Ma, C.; Matousek, P.; Parker, A. W.; Phillips, D.; Toner, W. T.; Towrie, M.; Umapathy, S. *J. Phys. Chem. A* **2001**, *105*, 984−990.
(17) Kwok, W. M.; Ma, C.; Parker, A. W.; Phillips, D.; Towrie, M.; Matousek, P.; Phillips, D. L. *J. Chem. Phys*. **2000**, *113*, 7471−7478.
(18) Dym, S.; Hochstrasser, R. M. *J. Chem. Phys*. **1969**, *51*, 2458−2468.
(19) Wagner, P. J.; Kemppainen, A. E.; Schott, H. N. *J. Am. Chem. Soc.* **1973**, *95*, 5604−5614.
(20) Lutz, H.; Breheret, E.; Lindqvist, L. *J. Phys. Chem*. **1973**, *77*, 1758−1762.
(21) Wagner, P. J.; Truman, R. J.; Scaiano, J. C. *J. Am. Chem. Soc.* **1985**, *107*, 7093−7097.
(22) (a) Myers, A. B.; Mathies, R. A. In *Biological Applications of Raman Spectroscopy*; Spiro, T. G., Ed.; Wiley: New York, 1987; Vol. 2, p 1. (b) Myers, A. B. In *Laser Techniques in Chemistry*; Myers, A. B., Rizzo, T. R., Eds.; Wiley: New York, 1995; p 325. (c) Myers, A. B. *Chem. Rev.* **1996**, *96*, 911−926.
(23) Ci, X. P.; Myers, A. B. *Chem. Phys. Lett*. **1989**, *158*, 263−270.
(24) Phillips, D. L.; Myers, A. B. *J. Chem. Phys.* **1991**, *95*, 226−243.
(25) Waterland, M. R.; Kelley, A. M. *J. Phys. Chem. A* **2001**, *105*, 8385−8392.
(26) Leng, W. A.; Kelley, A. M. *Langmuir* **2003**, *19*, 7049−7055.
(27) Tauber, M. J.; Mathies, R. A. *J. Phys. Chem. A* **2001**, *105*, 10952−10960.
(28) Tauber, M. J.; Mathies, R. A. *J. Am. Chem. Soc.* **2003**, *125*, 1394−1402.
(29) (a) Webb, M. A.; Loppnow, G. R. *J. Phys. Chem. A* **1999**, *103*, 6283−6287. (b) Webb, M. A.; Loppnow, G. R. *J. Phys. Chem. B* **2002**, *106*, 2102−2108.
(30) Fraga, E.; Loppnow, G. R. *J. Phys. Chem. B* **2002**, *106*, 10474−10481.
(31) Reid, P. J. *Acc. Chem. Res.* **2001**, *34*, 691−698.
(32) (a) Reid, P. J. *J. Phys. Chem. A* **2002**, *106*, 1473−1482. (b) Barham, B. P.; Reid, P. J. *Chem. Phys. Lett.* **2002**, *361*, 49−56.
(33) Reid, P. J.; Loftus, C.; Beeson, C. C. *Biochemistry* **2003**, *42*, 2441−2448.
(34) (a) Biswas, N.; Umapathy, S. *J. Chem. Phys.* **1997**, *107*, 7849−7858. (b) Biswas, N.; Abraham, B.; Umapathy, S. *J. Phys. Chem. A* **2002**, *106*, 9397−9406. (c) Biswas, N.; Umapathy, S. *J. Chem. Phys.* **2003**, *118*, 5526−5536.
(35) (a) Zhong, Y. P.; McHale, J. L. *J. Chem. Phys.* **1997**, *107*, 2920−2929. (b) Cao, X.; McHale, J. L. *J. Chem. Phys.* **1998**, *109*, 1901−1911. (c) McHale, J. L. *Acc. Chem. Res.* **2001**, *34*, 265−272.
(36) (a) Kwok, W. M.; Phillips, D. L. *J. Chem. Phys.* **1996**, *104*, 2529−2540. (b) Kwok, W. M.; Philliips, D. L. *J. Chem. Phys.* **1996**, *104*, 9816−9832. (c) Man, S. Q.; Kwok, W. M.; Johnson, A. E.; Phillips, D. L. *J. Chem. Phys.* **1996**, *105*, 5842−5857.
(37) (a) Zheng, X.; Phillips, D. L. *J. Chem. Phys.* **1998**, *108*, 5772−5783. (b) Zheng, X.; Phillips, D. L. *J. Chem. Phys.* **1999**, *110*, 1638−1649. (c) Zheng, X.; Lee, C. W.; Phillips, D. L. *J. Chem. Phys.* **1999**, *111*, 11034−11043.
(38) (a) Kwok, W. M.; Phillips, D. L.; Yeung, P. K. Y.; Yam, V. W. W. *J. Phys. Chem. A* **1997**, *101*, 9286−9295. (b) Leung, K. H.; Phillips, D. L.; Tse, M. C.; Che, C. M.; Miskowski, V. M. *J. Am. Chem. Soc.* **1999**, *121*, 4799−4803. (c) Xia, B. H.; Zhang, H. X.; Che, C. M.; Leung, K. H.; Phillips, D. L.; Zhu, N.; Zhou, Z. Y. *J. Am. Chem. Soc.* **2003**, *125*, 10362−10374.

(39) (a) Heller, E. J. *J. Chem. Phys.* **1975**, *62*, 1544. (b) Lee, S. Y.; Heller, E. J. *J. Chem. Phys.* **1979**, *71*, 4777. (c) Heller, E. J.; Sundberg, R. L.; Tannor, D. J. *J. Phys. Chem.* **1982**, *86*, 1822.
(40) Ziegler, L. D.; Hudson, B. *J. Chem. Phys.* **1981**, *74*, 982.
(41) (a) Ziegler, L. D.; Albrecht, A. C. *J. Chem. Phys.* **1979**, *70*, 2644. (b) Ziegler, L. D.; Albrecht, A. C. *J. Chem. Phys.* **1979**, *70*, 2634.
(42) Ziegler, L. D.; Hudson, B. *J. Chem. Phys.* **1983**, *79*, 1197.
(43) Ziegler, L. D.; Hudson, B. *J. Chem. Phys.* **1983**, *79*, 1134.
(44) Li, B.; Myers, A. B. *J. Phys. Chem.* **1990**, *94*, 4051.
(45) Choi, C. L.; Cheng, Y. F.; Yip, C.; Phillips, D. L.; Yam, V. W. W. *Organometallics.* **2000**, *19*, 3192.
(46) Cheng, Y. F.; Phillips, D. L.; He, G. Z.; Che, C. M.; Chi, Y. *Chem. Phys. Lett.* **2001**, *338*, 308.
(47) Frisch, M. J.; Trucks, G. W.; Schlegel, H. B.; Scuseria, G. E.; Robb, M. A.; Cheeseman, J. R.; Zakrzewski, V. G.; Montgomery, J. A., Jr.; Stratmann, R. E.; Burant, J. C.; Dapprich, S.; Millam, J. M.; Daniels, A. D.; Kudin, K. N.; Strain, M. C.; Farkas, O.; Tomasi, J.; Barone, V.; Cossi, M.; Cammi, R.; Mennucci, B.; Pomelli, C.; Adamo, C.; Clifford, S.; Ochterski, J.; Petersson, G. A.; Ayala, P. Y.; Cui, Q.; Morokuma, K.; Malick, D. K.; Rabuck, A. D.; Raghavachari, K.; Foresman, J. B.; Cioslowski, J.; Ortiz, J. V.; Stefanov, B. B.; Liu, G.; Liashenko, A.; Piskorz, P.; Komaromi, I.; Gomperts, R.; Martin, R. L.; Fox, D. J.; Keith, T.; Al-Laham, M. A.; Peng, C. Y.; Nanayakkara, A.; Gonzalez, C.; Challacombe, M.; Gill, P. M. W.; Johnson, B. G.; Chen, W.; Wong, M. W.; Andres, J. L.; Head-Gordon, M.; Replogle, E. S.; Pople, J. A. *Gaussian 98*, revision A.7; Gaussian, Inc.: Pittsburgh, PA, 1998.
(48) Silva, C. R.; Reilly, J. P. *J. Phys. Chem.* **1996**, *100*, 17111−17123.
(49) Catalan, J.; Mena, E.; Febero, F.; Amat-Guerri, F. *J. Chem. Phys.* **1992**, *96*, 2005−2016.
(50) Fang, W. H.; Phillips, D. L. *ChemPhysChem* **2002**, 889−892.
(51) Srivastava, S.; Yourd, E.; Toscano, J. P. *J. Am. Chem. Soc.* **1998**, *120*, 6173−6174.
(52) Sun, H.; Frei, H. *J. Phys. Chem. B* **1997**, *101*, 205−209.
(53) Tahara, T.; Hamaguchi, H.; Tasumi, M. *J. Phys. Chem.* **1990**, *94*, 170−178.
(54) Eijk, A. M. J.; Verhey, P. F. A.; Huizer, A. H.; Varma, C. A. G. O. *J. Am. Chem. Soc.* **1987**, *109*, 6635−6641.
(55) Hoffmann, R.; Swenson, J. R. *J. Phys. Chem.* **1970**, *74*, 415−420.
(56) Zwarich, R. J.; Goodman, L. *Chem. Phys. Lett.* **1970**, *7*, 609−611.
(57) Casida, M. E.; Jamorski, C.; Casida, K. C.; Salahub, D. R. *J. Chem. Phys.* **1998**, *108*, 4439−4449.
(58) Bauernschmitt, R.; Haser, M.; Treutler, O.; Ahlrichs, R. *Chem. Phys. Lett.* **1997**, *264*, 573−578.
(59) Bauernschmitt, R.; Ahlrichs, R. *Chem. Phys. Lett.* **1996**, *256*, 454−464.
(60) Our unpublished results.
(61) Weersink, R.; Wallace, S. C.; Gordon, R. D. *J. Chem. Phys.* **1995**, *103*, 9530−9540 and reference therein.
(62) Andrieux, C. P.; Saveant, J. M.; Tallec, A.; Tradivel, R.; Tardy, C. *J. Am. Chem. Soc.* **1996**, *118*, 9788−9789.
(63) McClelland, R. A.; Kanagasabapathy, V. M.; Steenken, S. *J. Am. Chem. Soc.* **1988**, *110*, 6913−6914.
(64) Cozens, F. L.; O'Nell, M.; Bogdanova, R.; Schepp, N. *J. Am. Chem. Soc.* **1997**, *119*, 10652−10659.
(65) Rentzepis, P. M. *Science* **1970**, *169*, 239−247.
(66) Berger, M.; Goldblatt, I. L.; Steel, C. *J. Am. Chem. Soc.* **1973**, *95*, 1717−1725.
(67) Berger, M.; Steel, C. *J. Am. Chem. Soc.* **1975**, *97*, 4817−4821.
(68) Turro, N. J. In *Modern Molecular Photochemistry*; Turro, N. J., Ed.; University Science Books: Mill Valley, CA, 1991; p 29.